Prototype Parallel Readout System for Position Sensitive PMT Based Gamma Ray Imaging Systems

Frezghi Habte, *Member, IEEE*, Peter D. Olcott, Craig S. Levin, *Member, IEEE*, and Angela M. Foudray, *Student Member, IEEE*

***Abstract*—A parallel prototype readout system that allows digitization and acquisition of 64 or more anode signals from a position sensitive photomultiplier tube (PSPMT) was developed for a miniature hand-held gamma camera. This acquisition system was developed to study the benefits of a digital readout system compared to charge multiplexed techniques such as resistive division. The system was developed using CAMAC instrumentation standard and controlled via a Macintosh Computer. Four 16-channel charge-to-digital conversion (QDC) CAMAC modules were used to digitize individual anode signals from the PSPMT. To maximize the data transfer rate, a list processor module was also added in the system. For acquisition and processing of the digitized data, we used Kmax software from SPARROW. The system provided 99.9% spatial linearity when inter-anode gain correction was applied to list-mode data. Much improved scintillation crystal separation in a flood histogram with 16:1 peak to valley ratio, and higher edge sensitivity was obtained compared to resistive charge multiplexing readout.**

***Index Terms*—CAMAC, data acquisition, digital-readout, gamma camera, lutetium oxyorthosilicate (LSO), position sensitive photomultiplier tube (PSPMT).**

I. Introduction

A miniature hand-held gamma camera is being developed for surgical cancer staging [1]. The camera studied in this paper is based upon a $5 \times 5\ \mathrm{cm}^2$ imaging field of view (FOV) flat-panel position sensitive photomultiplier tube (PSPMT) and discrete LSO (lutetium oxy-orthosilicate) scintillation crystal array. Due to high signal-to-noise ratio, PSPMTs are the most common photodetectors used in many imaging applications ranging from compact imaging probes to small animal PET scanners [2]–[8].

Typically, the readout of PSPMT based detector systems are performed using a resistive charge division technique [9]–[14] as it provides a relatively simple electronics solution. On the other hand, the non-uniform spatial response and gain variation of a PSPMT within a small field-of-view (FOV) camera significantly degrades performance unless individual anode correction is applied. As reported in [15] a charge division based readout system has limitations in accurate localization of events and can cause resolution degradation. The edge effects inherent to this method also limit the useful FOV.

The main advantage of independent channel readout is that it allows digital correction of gain variation, cross-talk and non-uniformity within the readout channels providing more accurate position estimation and superior image quality. A drawback is that it requires more supporting electronics. However due to the advances and novel developments in the technology of digitizer chips and integrated circuits, this is no longer a great impediment. Another limitation, especially when using large number of channels is that it requires high bandwidth to maintain acceptable count rate, which may not be supported with current technology. A dedicated custom design of an interface bus that combines parallel sampling with digital multiplexing may be required.

This work focuses on the development of a prototype multi-channel readout system to study the advantages of a parallel readout system compared to charge multiplexing techniques.

II. Materials and Methods

A. Readout System Description

Our compact gamma camera uses the Hamamatsu H8500 flat-panel PSPMT detector equipped with 64 (8×8) anode pixels in a $50 \times 50\ \mathrm{mm}^2$ square detector area. This detector is coupled to a configuration of collimator and scintillation crystal array optimized for photon detection sensitivity and resolution. The signal output from each PSPMT anode is read out individually using a CAMAC based acquisition system as depicted in Fig. 1. Four modules of charge-to-digital converters (QDCs) (Phillips Scientific model 7166), each with 16-channels are used to simultaneously digitize the signals from all 64 channels of the PSPMT detector for each event. The signal from the last dynode is inverted and used to generate a fast gate signal to trigger the acquisition of an event in the QDCs. The delay between the analog input signals and gate signal was adjusted using an in-house delay board built from discrete delay components. Since the gain of the PSPMT provided detectable signal ($\sim$200 mV signal amplitude) above the noise floor and within the dynamic range of the QDC (-512 pC full scale in 12 bit range), the delayed analog signals are coupled directly to the QDC inputs without amplification or shaping the signal. The input charge from each anode within the QDC is integrated and

Manuscript received November 24, 2003; revised August 11, 2005. This work was supported by the Whitaker Foundation under Research Grant RG-01-0492.

F. Habte was with the Department of Radiology, Stanford University, Stanford, CA 94305-5344 USA. He is now with Oak Ridge National Laboratory, Oak Ridge, TN 37831 USA (e-mail: fhabte@ornl.gov).

P. D. Olcott and C. S. Levin are with the Department of Radiology, Stanford University, Stanford, CA 94305-5344 USA (e-mail: pdo@stanford.edu; cslevin@stanford.edu).

A. M. Foudray is with the Physics Department, University of California, San Diego, San Diego, CA 92037 USA and also with the Department of Radiology, Stanford University, Stanford, CA 94305-5344 USA (e-mail: afoudray@stanford.edu).

Color versions of one or more of the figures in this paper are available online at http://ieeexplore.ieee.org.

Digital Object Identifier 10.1109/TNS.2006.889157

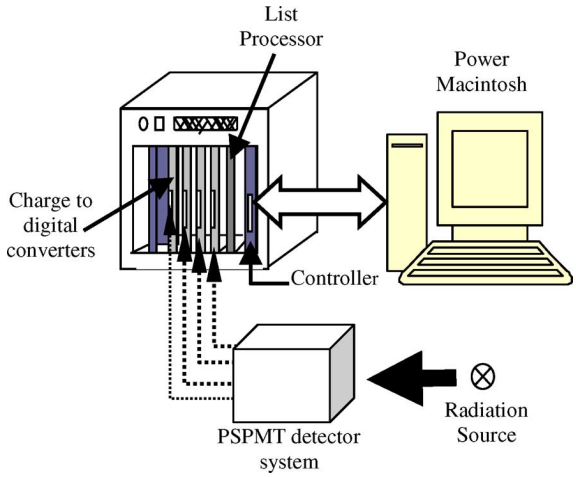

Fig. 1. Experimental setup of CAMAC based a parallel readout and acquisition system.

digitized in parallel to register an event. The integration time is determined by the gate width, which can be adjusted to an optimal signal to noise ratio (∼40 dB) using a Co-57 gamma source.

Each QDC requires a minimum of 7.2 μs conversion time, which is relatively small compared to the long reading cycle of the CAMAC system (∼100 ms/channel). To maximize the data rate a list processor (Hytec Electronics LP 1342) is included in the readout system. We are able to read and transfer the QDC digitized data to the list processor data buffer in about 1.5 μs per channel (a total of 96 μs for 64 channels). This limits the sampling rate of the system to 9.6 kHz, yielding a maximum data rate of 1.3 Mbytes/s. The digital data is transferred in real time to a G4 power Mac via SCSI bus Controller (Jorway 73A), which allows maximum throughput of 2 Mbytes/s.

B. Software Implementation

The digitized data is acquired and processed in a Mac using Kmax [16], a simplified built-in script based programming language from SPARROW Co., which significantly simplified the software implementation. Kmax allows non-buffered (event by event) or buffered acquisition options. In either case, the event is acquired and sorted in real-time and/or saved in list mode data for off-line processing. In order to simultaneously sample the event from four QDC modules and reduce the reading cycle, a global clear signal is applied that clears the QDC modules after each event is read out. This signal is generated from a dataway display CAMAC module. The list mode data is processed off-line using Matlab. Event positioning was performed by calculating centroid coordinates using a weighted mean algorithm as described below:

$$x_{pos} = \frac{\sum_{i=1}^{8}\left(\sum_{j=1}^{8} a_{ij}\right)\bullet i}{\sum_{k=1}^{64} a_k}, \quad \text{and} \quad y_{pos} = \frac{\sum_{j=1}^{8}\left(\sum_{i=1}^{8} a_{ij}\right)\bullet j}{\sum_{k=1}^{64} a_k}$$

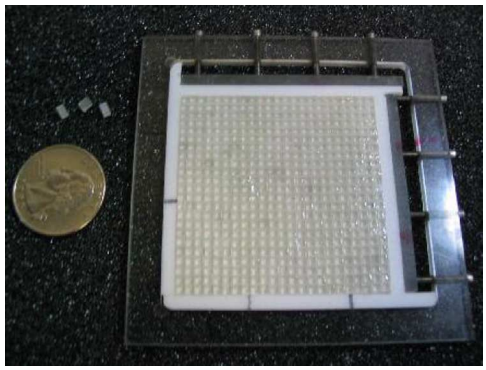

Fig. 2. A 23 × 23 LSO crystal array of each $2 \times 2 \times 3\ \mathrm{mm}^3$ forming a total LSO volume of $50 \times 50 \times 3\ \mathrm{mm}^3$.

where x_{pos} and y_{pos} are the centroid coordinates. a_{ij} and a_{k} are individual anode signals (energies) recorded for each event.

C. Measurements

The gain of each anode of the PSPMT detector may vary due to factors such as the lifetime of the PSPMT, the biasing voltage used and readout electronics of the specific experimental set up. In order to apply a highly accurate gain correction to our flood measurements, gain variation of the PSPMT detector within the 64 anodes was measured using the prototype readout systems and a green LED light source at a distance of 40 cm from the face of the PSPMT. For this measurement, the list mode data from all anode signals were acquired and sorted according to anode pulse heights. Gain variation was determined from the peak location in the pulse height of all 64-anode signals and was normalized to the maximum anode signal for display.

For absorption of photons, a 23 × 23 LSO crystal array is formed from crystal elements, each $2 \times 2 \times 3\ \mathrm{mm}^3$ (Fig. 2). We used four layers of Teflon tape to cover each crystal face except the side coupled to the PSPMT. The resulting reflector thickness is estimated to be 0.15 mm between adjacent crystals. The crystal array was coupled to the PSPMT using silicon optical grease. The detector system was flood irradiated using a $^{57}\mathrm{Co}$ source (122 keV) without collimator.

We measured crosstalk between adjacent anodes and light distribution shared between neighboring anodes using a single LSO crystal $(2 \times 2 \times 3\ \mathrm{mm}^3)$ placed in several positions on the PSPMT (Fig. 5, middle column). For each crystal location, we recorded the digitized list-mode data from all anodes simultaneously. A distribution of positioned events was generated from 2000 events that were acquired for each crystal location.

In order to perform an inter-crystal cross talk measurement, a 5 × 5 LSO array of $2 \times 2 \times 3\ \mathrm{mm}^3$ individual crystals was coupled to the center of the PSPMT using optical grease. Four layers of Teflon tape covered each crystal except the side coupled to the PSPMT. The center crystal in the 5 × 5 LSO crystal array was irradiated through a collimated source with spot size of 0.7 mm using a $^{57}\mathrm{Co}$ point source (122 keV). List mode data was recorded from 16 central anodes covering the crystal array.

Energy resolution for each of the 64 anodes of the PSPMT was measured using a single LSO crystal directly coupled to

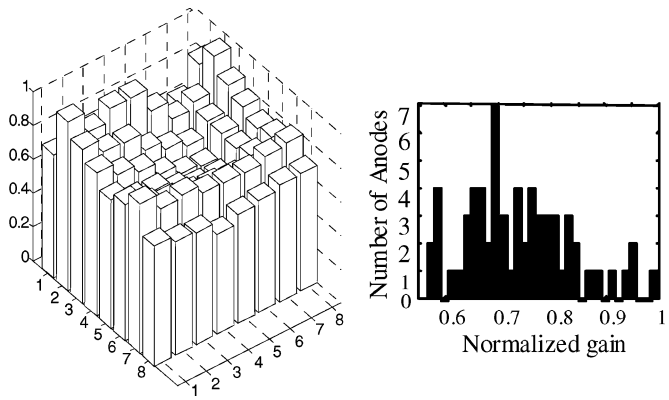

Fig. 3. Left: normalized gain variation map for 64 anodes measured from flood irradiation using an LED light source. Right: the anode gain histogram.

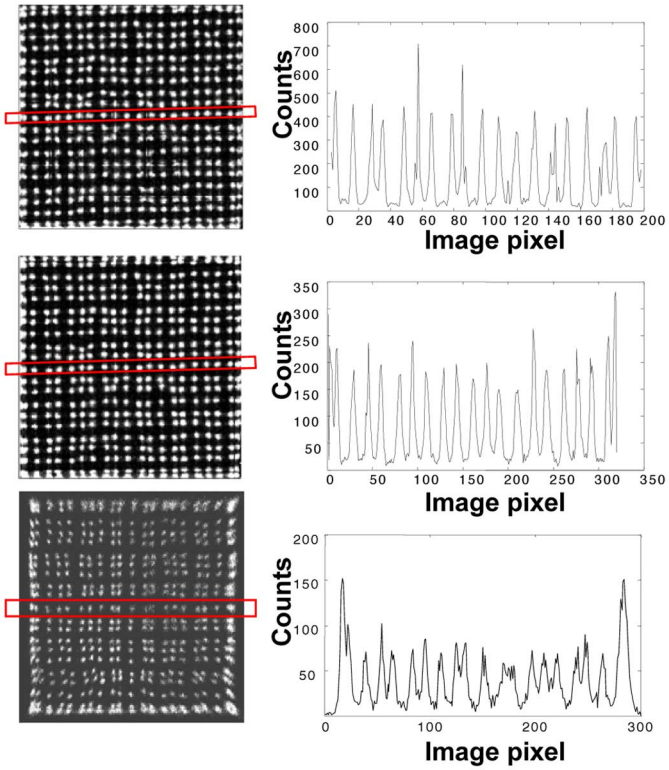

Fig. 4. Top row: flood images and cross section profile across central row for 23 × 23 LSO crystal array obtained using parallel readout before gain correction is applied. Middle row: corresponding data using parallel readout after gain correction is applied. Bottom row: flood measurements for 23 × 23 LSO crystal array and cross section profile across central row obtained using resistive charge multiplexing readout [17].

the center of each PSPMT anode. The energy spectrum obtained from one anode, sum of 9 anodes and sum of all 64 anodes of the PSPMT were compared. To measure the spatial resolution of the detector system, we stepped a collimated source of ^{57}Co with beam spot size ∼0.7 mm in steps of 0.4 mm across the middle row of the 5 × 5 array of 2 × 2 × 3 mm^3 LSO crystals coupled to the center of the PSPMT.

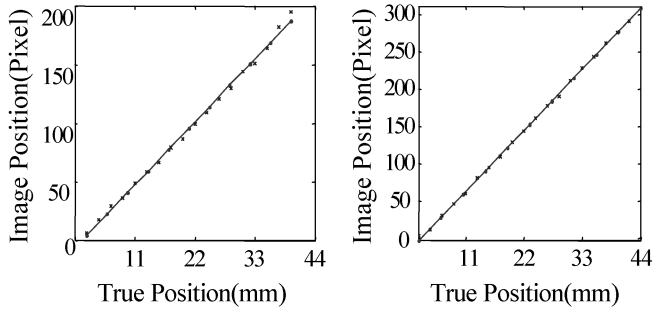

Fig. 5. Left: linearity curve: true crystal location vs. image location across the central row using parallel readout before gain correction is applied. Right: linearity curve after gain correction is applied.

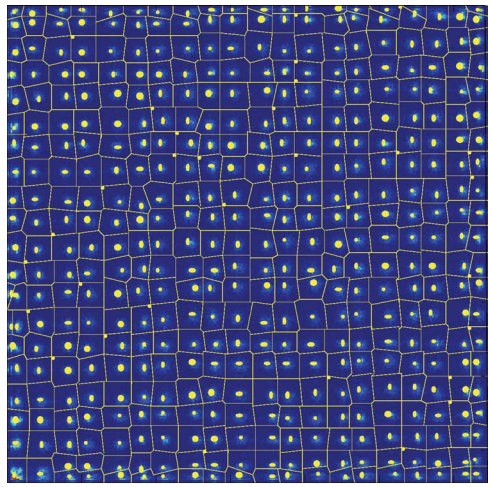

Fig. 6. Flood image segmentation map corresponding to crystal peak locations determined by drawing boundaries around each peak.

III. Results

A. Gain Variation Profile

Fig. 3 shows the histogram of gain variation, which was determined from recording the peak location in the pulse height spectrum for each anode. The data is normalized to the maximum anode signal for display. The maximum gain variation between anodes was roughly 45%. The measured gain map allowed the creation of a highly accurate gain correction that was applied to list mode data.

B. Flood Image, Linearity and Crystal Identification

Fig. 4 (Top and Middle rows) shows the crystal flood histogram and cross-section profile through the central row using parallel readout with and without gain correction respectively. For comparison, Fig. 4 (Bottom row) also shows a flood image obtained using a new advance resistive charge multiplexed readout technique developed in our lab [17]. Note that no energy discrimination or image processing has been applied to the raw flood images shown. Compared to resistive charge multiplex readout (∼7:1 average peak to valley ratio), the parallel readout provided better image quality with 13:1 average peak to valley ratio. All crystals (∼ 21 × 21 crystals) within the active FOV of the PSPMT are visible, with the positioning dynamic range extending to the FOV edges. Due to non-linear behavior

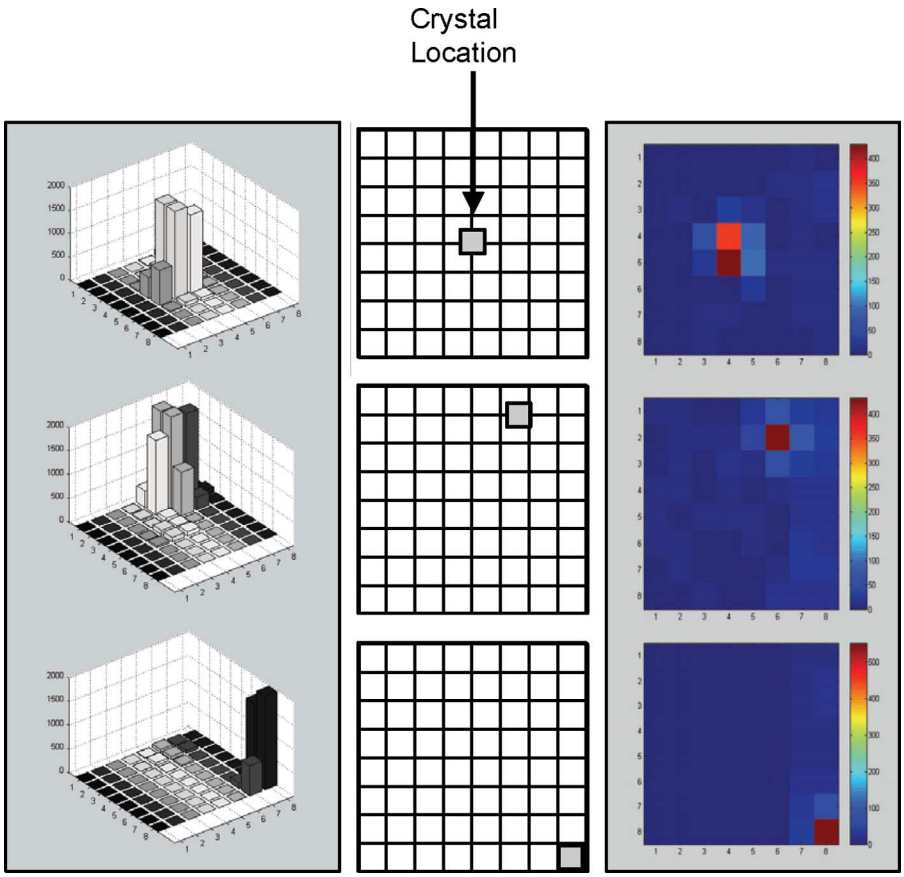

Fig. 7. Cross-talk measurements. Left: histogram of positioned events recorded. Middle: crystal location. Right: light spread for single event.

at the edge of the PSPMT FOV, the edge of the positioning dynamic range is compressed and the edge crystals are shifted slightly inwards in the flood image. In the case of the resistive charge multiplexing technique, relatively large edge crystal distortions and compressed positioning dynamic range are observed. Spatial linearity, measured from plotting the true vs. mapped crystal position was excellent for the parallel readout scheme with correlation coefficient $R^2 > 99\%$ (Fig. 5, Left). The improved resistive charge multiplex readout also provided similar linearity performance [17].

After gain correction is applied, both the crystal identification and the linearity of the flood histogram were improved. An average peak to valley ratio of 16:1 was obtained with similar image distortion compared to that observed before gain correction. After gain correction, a slightly higher degree of spatial linearity ($R^2 > 99.9\%$) was also observed as shown in Fig. 5.

Fig. 6 shows the crystal positioning look-up map, which was determined by drawing boundaries around the crystal peak locations in the flood image using a minimum distance to peak algorithm [18]. This crystal segmentation is used to extract individual crystal counts, average pulse height per crystal, and energy resolution from each crystal for detailed evaluation and calibration of the detector system. This segmented map may also be used to generate lookup tables to correct spatial linearity and uniformity and to perform event energy discrimination over the array.

C. Inter Anode Cross Talk and Light Distribution

Fig. 7, Left column shows a distribution of positioned events for a single LSO crystal placed at three different locations on the face of the PSPMT showing the cross talk between adjacent anodes and the light distribution within the neighboring anodes. We also analyzed the distribution of anode signals recorded for just one gamma ray event in the list (Fig. 7, Right column). In all cases event positioning and light distribution are highly localized; At most 9 anodes are involved in the light collection and positioning for any event. The anodes for which part or all of their active area is optically coupled to the LSO crystal recorded more than 95% of the available light signal from gamma ray events.

D. Inter-Crystal Cross Talk and LSO Background

A 2D event positioning histogram was formed from the recorded events when the central crystal in a 5×5 LSO crystal array placed at the center of the PSPMT was irradiated using a collimated source (Fig. 8, Left). Counts from each crystal were extracted from a positioning look up map after crystal segmentation was applied (see Fig. 6). The results (Fig. 8, Right) show the count distribution over the array. There is $<$ 6% cross talk with the immediate neighbor crystals. Note also that some of the counts seen in other crystals are due to the LSO background, which is less than 2.5 cps/crystal [1], [17],

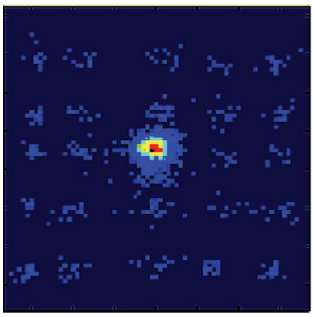

50	45	65	50	62
51	52	98	67	64
51	97	2415	56	48
47	68	148	57	58
71	60	95	62	72

Fig. 8. Inter-crystal cross talk measurement. A center crystal in 5 × 5 array is irradiated using a collimated source. Left: resulting 2D image of 5 × 5 crystal array. Right: number of events recorded in each crystal.

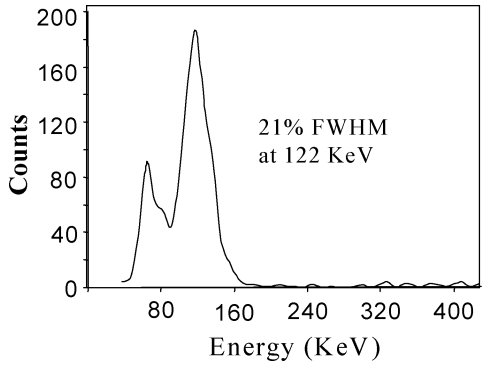

Fig. 9. Sample ^{57}Co energy spectra for a single $2 \times 2 \times 3$ mm^3 LSO crystal coupled to a single anode.

[19], [20], which has not been subtracted from this data set. In this measurement, about 3% LSO background was recorded from the irradiated central crystal.

E. Energy Resolution

The single anode energy spectrum is shown in Fig. 9 for a typical LSO crystal coupled to one PSPMT anode. The energy resolution, measured by a Gaussian fit to the 122 keV photopeak for the 23 × 23 array, ranges from 21% to 29% with an average value of 25% FWHM. The energy resolution was similar within error bars using the single anode with maximum signal or when nine nearest neighbor anodes are summed and gain correction is applied to each anode. However, the energy resolution was ∼5% worse when all 64 anodes with gain correction are summed to determine energy. This is due to the integration of noise in all anodes and the small pedestal variation (∼1%) among the QDC channels.

For comparison, individual energy spectra were also extracted for 30 central crystals selected from the flood image shown in Fig. 6 as extracted from the segmented flood map. The calculated single crystal energy resolution ranged from 27% to 34% with average value of 30% over the 30 crystals. This is slightly worse than for the case of single crystal coupled to a single anode since for the array, light from any one crystal is shared between multiple anodes and may be lost in dead spaces of the PSPMT before reaching to the anodes. In addition, inter-crystal scatter occurs for the crystal array.

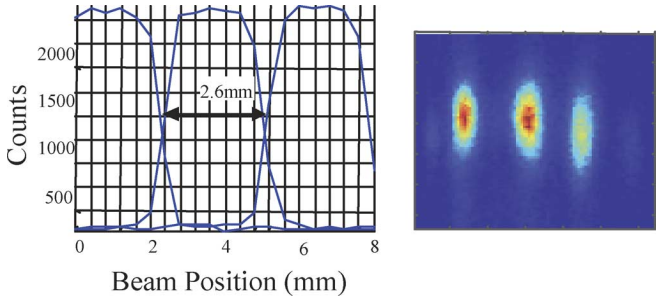

Fig. 10. Left: spatial resolution profiles measured through three central crystals with a 0.7 mm wide photon ^{57}Co beam. Right: resulting sum image from traversing three crystals.

F. Spatial Resolution

Fig. 10 shows, the result of scanned collimated source across the middle row of the 5 × 5 crystal array at the center of the PSPMT for spatial resolution measurements. A raw spatial resolution of approximately 2.6 mm FWHM was obtained. Deconvolving the beam spot (∼0.7 mm) aperture, gives 2.5 mm FWHM.

IV. Summary and Conclusion

We developed a parallel readout system that allows simultaneous digitization and acquisition of 64 detector signals from a multi-anode PSPMT based detector system. Although we have focused our development on reading out a PSPMT, the system may be used for variety of imaging applications. The capability of digital control per channel allowed accurate gain calibration and correction that allows one to optimize flood histogram image quality and spatial linearity. It also helped to perform detailed measurements of PSPMT characteristics such as inter-anode and inter-crystal cross talk and individual crystal energy resolution, which were useful for evaluation of the detector system.

A parallel readout system provides better performance since it does not introduce distortion as in the case of resistive division due to resistive elements. The limitation is that CAMAC based data acquisition is very slow, resulting in relatively low event count rate. The count rate performance of the system could be improved by applying a sparse readout method. In this method, any nine anodes above threshold within the localized LSO light cone was be read for event position estimation. A spatial resolution of 2.5 mm fwhm was obtained. Excellent crystal flood image quality with superior 16:1 peak to valley ratio was also obtained after gain correction.

References

[1] A. P. Dhanasopon, C. S. Levin, A. M. Foudray, P. D. Olcott, and F. Habte, "Scintillation crystal design features for a miniature gamma ray camera," *IEEE Trans. Nucl. Sci.*, vol. 52, no. 5, pp. 1439–1446, Oct. 2005.

[2] R. Pani *et al.*, "A novel compact gamma camera based on flat panel PMT," *Nucl. Instrum. Methods Phys. Res. A*, vol. A513, pp. 36–41, 2003.

[3] S. V. Gurus, Z. He, D. K. Wehe, and G. F. Knoll, "A portable gamma camera for radiation monitoring," *IEEE Trans. Nucl. Sci.*, vol. 42, no. 4, pp. 940–945, Aug. 1995.

[4] C. S. Levin, "Detector design issues for compact nuclear emission cameras dedicated to breast imaging," *Nucl. Instrum. Methods Phys. Res. A*, vol. A497, 2003.

[5] N. Gkanatsios *et al.*, "A portable CAMAC LabView nuclear medicine imagin system," *Physica Medica*, vol. IX, no. 2–3, Apr.–Sep. 1993.
[6] J. Vaquero *et al.*, "Performance characteristics of a compact position-sensitive LSO detector," *IEEE Trans. Med. Imag.*, vol. 17, no. 6, pp. 967–978, Dec. 1998.
[7] G. K. Loudos *et al.*, "Improving spatial resolution in SPECT with the combination of PSPMT based detector and iterative reconstruction algorithms," *Comput. Med. Imaging Graph.*, vol. 27, pp. 307–313, 2003.
[8] R. Pani, A. Soluri, R. Scafe, A. Pergola, R. Pelegrini, G. De Vincentis, G. Trotta, and F. Scopinaro, "Multi-PSPMT scintillation camera," *IEEE Trans. Nucl. Sci.*, vol. 46, no. 3, pp. 702–708, Jun. 1999.
[9] N. Zhang and C. J. Thompson, "Optimizing position readout circuits in positron emission tomography front-end electronics," *IEEE Trans. Nucl. Sci.*, vol. 50, no. 5, pp. 1398–1403, Oct. 2003.
[10] A. Pullia, W. F. J. Muller, C. Boiano, and R. Bassini, "Resistive or capacitive charge-division readout for position-sensitive detectors," *IEEE Trans. Nucl. Sci.*, vol. 49, no. 6, pp. 3269–3277, Dec. 2002.
[11] C. M. Laymon, R. S. Miyaoka, B. K. Park, and T. K. Lewellen, "Simplified FPGA-based data acquisition system for PET," *IEEE Trans. Nucl. Sci.*, vol. 50, no. 5, pp. 1483–1486, Oct. 2003.
[12] S. Siegel, R. W. Silverman, Y. Shao, and S. R. Cherry, "Simple charge division readouts for imaging scintillator arrays using a multi-channel PMT," *IEEE Trans. Nucl. Sci*, vol. 43, no. 3, pp. 1634–1641, Jun. 1996.
[13] J. L. Alberi and V. Radeka, "Position sensing by charge division," *IEEE Trans. Nucl. Science*, vol. 23, no. 1, pp. 251–258, Feb. 1976.
[14] R. L. Clancy, C. J. Thompson, J. L. Robar, and A. M. Bergman, "A simple technique to increase the linearity and field-of-view in position sensitive photomultiplier tubes," *IEEE Trans. Nucl. Sci.*, vol. 44, no. 3, pp. 494–498, Jun. 1997.
[15] R. Pani *et al.*, "Flat panel PMT for photon emission imaging," *Nucl. Instrum. Methods Phys. Res. A*, vol. A505, pp. 590–594, 2003.
[16] Sparrow Corporation. Daytona Beach, FL.
[17] P. D. Olcott, J. A. Talcott, C. S. Levin, F. Habte, and A. M. K. Foudray, "Compact readout electronics for position sensitive photomultiplier tubes," *IEEE Trans. Nucl. Sci.*, vol. 52, no. 1, pp. 21–27, Feb. 2005.
[18] C. B. Barber, D. P. Dobkin, and H. T. Huhdanpaa, "The quickhull algorithm for convex hulls," *ACM Trans. Math. Softw.*, vol. 22, no. 4, pp. 469–483, Dec. 1996.
[19] J. S. Huber, W. W. Moses, W. F. Jones, and C. C. Watson, "Effect of 176Lu background on singles transmission for LSO-based PET cameras," *Phys. Med. Biol.*, vol. 47, pp. 3535–3541, 2002.
[20] C. L. Melcher and J. S. Schweitzer, "Cerium-doped lutetium oxyorthosilicate: a fast, efficient new scintillator," *IEEE Trans. Nucl. Sci.*, vol. 39, no. 4, pp. 502–505, Aug. 1992.